Title

Spatially variable water table recharge and the hillslope hydrologic response: Analytical solutions to the linearized hillslope Boussinesq equation

Journal

Water Resources Research, 50(11)

ISSN

0043-1397

Authors

Dralle, David N
Boisramé, Gabrielle FS
Thompson, Sally E

Publication Date

2014-11-01

DOI

10.1002/2013wr015144

Peer reviewed

AGU PUBLICATIONS

Water Resources Research

RESEARCH ARTICLE
10.1002/2013WR015144

Key Points:
- To derive new analytical solutions in hydraulic groundwater theory
- Spatially variable recharge alters hillslope base flow discharge properties
- Spatially variable recharge alters the hydrologic effects of topography

Supporting Information:
- Readme
- Validation of analytical solutions

Correspondence to:
D. N. Dralle,
dralle@berkeley.edu

Citation:
Dralle, D. N., G. F.S. Boisramé, and S. E. Thompson (2014), Spatially variable water table recharge and the hillslope hydrologic response: Analytical solutions to the linearized hillslope Boussinesq equation, *Water Resour. Res.*, *50*, 8515–8530, doi:10.1002/2013WR015144.

Received 3 DEC 2013
Accepted 16 SEP 2014
Accepted article online 19 SEP 2014
Published online 7 NOV 2014

Spatially variable water table recharge and the hillslope hydrologic response: Analytical solutions to the linearized hillslope Boussinesq equation

David N. Dralle[1], Gabrielle F.S. Boisramé[1], and Sally E. Thompson[1]

[1]Department of Civil and Environmental Engineering, University of California, Berkeley, California, USA

Abstract The linearized hillslope Boussinesq equation, introduced by *Brutsaert* (1994), describes the dynamics of saturated, subsurface flow from hillslopes with shallow, unconfined aquifers. In this paper, we use a new analytical technique to solve the linearized hillslope Boussinesq equation to predict water table dynamics and hillslope discharge to channels. The new solutions extend previous analytical treatments of the linearized hillslope Boussinesq equation to account for the impact of spatiotemporal heterogeneity in water table recharge. The results indicate that the spatial character of recharge may significantly alter both steady state subsurface storage characteristics and the transient hillslope hydrologic response, depending strongly on similarity measures of controls on the subsurface flow dynamics. Additionally, we derive new analytical solutions for the linearized hillslope-storage Boussinesq equation and explore the interaction effects of recharge structure and hillslope morphology on water storage and base flow recession characteristics. A theoretical recession analysis, for example, demonstrates that decreasing the relative amount of downslope recharge has a similar effect as increasing hillslope convergence. In general, the theory suggests that recharge heterogeneity can serve to diminish or enhance the hydrologic impacts of hillslope morphology.

1. Introduction

The hillslope Boussinesq (HB) equation forms a key component of hydraulic groundwater theory. It describes the spatiotemporal evolution of a slowly draining water table along a one-dimensional hillslope, allowing storage and discharge from the hillslope to be estimated at any point in time. The HB is derived under the assumption that saturated subsurface flow occurs purely parallel to an impermeable bottom boundary (the hydrostatic assumption), that the effects of capillarity can be lumped into the water table evolution (an assumption reflected in the use of the 'drainable porosity parameter', n_e, rather than the true porosity, n, when computing mass balances in the subsurface [*Hilberts et al*., 2007]), and that a net recharge parameter, $R(x,t)$, can be specified to account for the effects of both vertical infiltration from the surface to the water table and losses of water due to evaporation and root uptake in the unsaturated zone [*Brutsaert*, 2005]. These conditions and their outcomes are illustrated in Figure 1.

With these assumptions, Darcy's Law can be combined with the mass continuity equation to obtain HB as the governing partial differential equation for a homogeneous, unconfined aquifer set above a sloping impermeable layer:

$$\frac{\partial \eta}{\partial t} = \frac{k_0 \cos\theta}{n_e}\frac{\partial}{\partial x}\left(\eta\frac{\partial \eta}{\partial x}\right) + \frac{k_0 \sin\theta}{n_e}\frac{\partial \eta}{\partial x} + \frac{R(x,t)}{n_e}. \quad (1)$$

Here η [L] is the height of the water table above the impermeable layer in the sloping reference frame, k_0 [L/T] is the hydraulic conductivity, n_e is the drainable porosity, θ is the slope angle of the underlying impermeable layer, and $R(x, t)$ [L/T] is a source term representing any recharge to the water table.

No general analytical solutions are known for the full HB, although a limited set of solutions are available through approximation methods [*Boussinesq*, 1877; *Polubarinova-Kochina*, 1962]. To progress toward a more generalizable solution method, *Brutsaert* [1994] linearized (1) by expanding the diffusive term:

$$\frac{\partial}{\partial x}\left(\eta\frac{\partial \eta}{\partial x}\right) = \left(\frac{\partial \eta}{\partial x}\right)^2 + \eta\frac{\partial^2 \eta}{\partial x^2}, \quad (2)$$

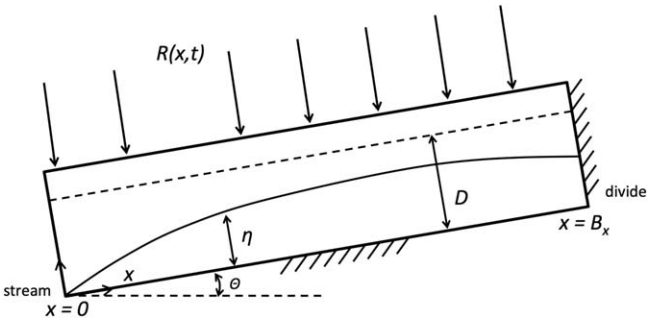

Figure 1. One-dimensional profile of a hillslope at angle θ with a water table height profile (η) and initial water table depth (D). Hillslope length (B_x) is defined along the hillslope axis (x) and the water table recharge (R) can vary in both space (x) and time (t) [after *Brutsaert*, 2005].

and noting that if η fluctuates locally around an average water table height (η_0) the term $\left(\frac{\partial \eta}{\partial x}\right)^2$ is negligibly small and η in the second term of (2) can be replaced with η_0. The linearized HB (LHB) is then given by:

$$\frac{\partial \eta}{\partial t} = \frac{k_0 \eta_0 \cos\theta}{n_e}\frac{\partial^2 \eta}{\partial x^2} + \frac{k_0 \sin\theta}{n_e}\frac{\partial \eta}{\partial x} + \frac{R(x,t)}{n_e}. \quad (3)$$

Equation (3) has been successfully used to develop minimalistic, physically based hydrologic models and base flow separation algorithms [*Pauwels et al*., 2002; *Huyck et al*., 2005; *Rupp et al*., 2009]. Here we extend the analytical treatment of equation (3). While existing solution methodologies [*Pauwels et al*., 2002; *Troch et al*., 2004; *Verhoest and Troch*, 2000; *Brutsaert*, 1994; *Troch et al*., 2013] assume spatially homogeneous recharge, the new solution method admits analytical solutions for spatiotemporally variable forcing. We are motivated by high quality, remotely sensed data that highlight spatial heterogeneity in the distribution of vegetation, which we hypothesize could introduce significant spatial variability in water balance partitioning. With this in mind, we set two aims for the study:

1. To apply a recently developed solution technique for the analytical solution of spatially forced advection-diffusion equations, such as the linearized hillslope Boussinesq equation;
2. To explore the potential effects of spatially variable water table recharge and hillslope morphology on the hillslope hydrologic response and to determine when the new solution can be used in topographically complex situations.

In pursuit of these aims, we first develop a novel solution for the linearized HB based on recently developed methods for solving advection-diffusion equations [*Guerrero et al*., 2009]. In addition to a spatiotemporally varying recharge term, the new methods do not require the use of Laplace transforms for solving the partial differential equations, leading to a simpler analytical formulation for the problem. The solution methodology is extended to also address the linearized hillslope-storage Boussinesq (LHSB) equation, which accounts for the effects of convergence or divergence in hillslope morphology on water table dynamics [*Troch et al*., 2003].

Following the development of new solutions to the LHB and the LHSB, we examine the impact of spatially heterogeneous water table recharge on: (i) instantaneous water table and base flow responses to pulse inputs of water; (ii) seasonal hillslope storage volumes and seasonal base flow recession behavior; and (iii) hillslope flow recession characteristics in topographically complex situations. Topographic complexity is an important control on patterns of hillslope discharge and should be considered, but the linearization of the HSB requires more approximations in comparison to the HB [*Woods et al*., 1997; *Troch et al*., 2003]. Accordingly, we provide a detailed error analysis of LHSB performance across a variety of hillslopes and recharge patterns.

All cases are explored in the context of seasonally dry climates (where the volume, persistence and profile of base flow is of critical ecological and anthropic importance), on hillslopes where discharge to the channel is dominated by saturated subsurface flow. Throughout the study we employ simple (smoothed and homogeneous) representations of hillslope geometry, hydraulic properties, seasonal climate dynamics and spatial changes in hillslope water table recharge. While we recognize that deviations from these idealized conditions could alter the details of the results presented, the simplified cases capture the critical features of seasonality, hillslope topography, and the possible effects of spatially variable vegetation on recharge fluxes.

2. Methods

Equation (3) is a linear, constant-coefficient, nonhomogeneous advection-diffusion equation (nonhomogeneous in this case means there exists a term in the PDE which is not proportional to the dependent variable

or its derivatives). It has been solved explicitly for a variety of cases, including a no-recharge case [*Brutsaert*, 1994], with constant recharge [*Verhoest and Troch*, 2000], and with temporally variable recharge conditions ($R(t)$) [*Pauwels et al*., 2002]. These solutions and the broad utility of the LHB model were recently reviewed [*Troch et al*., 2013]. To date, all solutions presented to the LHB rely on the use of Laplace Transforms. While useful, Laplace Transform based methods are complex to implement, and constrain the range of solutions that can be obtained.

Here we outline an alternative, simpler solution methodology which allows the development of a more general analytical solution to the LHB. The solution methodology is based on a change of variable followed by the use of the Generalized Integral Transform Technique [*Guerrero et al*., 2009; *Cotta*, 1993].

2.1. General Solution

We seek a general solution to (3) using the boundary conditions established by *Brutsaert* [1994]: (i) a no-flux boundary condition at the upslope boundary of the hillslope, corresponding to the presence of a groundwater divide, (ii) a water table height of zero at the stream, approximating the conditions that prevail at the boundary where a water table meets a shallow, upland stream [*Brutsaert*, 2005], and (iii) an initial condition that assumes a uniform water table depth above the bottom boundary along the entire hillslope. Mathematically, these conditions are:

$$\begin{aligned} &\text{stream boundary condition}: \quad \eta=0 \quad x=0 \quad t>0,\\ &\text{divide boundary condition}: \quad \eta_0\cos\theta\frac{\partial\eta}{\partial x}+\eta\sin\theta=0 \quad x=B_x \quad t>0,\\ &\text{initial condition}: \quad \eta=D \quad 0\le x\le B_x \quad t=0. \end{aligned} \tag{4}$$

Following *Brutsaert* [2005], we nondimensionalize the variables with the following scalings:

$$x_+=\frac{x}{B_x}; \quad t_+=\frac{k_0\eta_0\cos\theta}{n_e{B_x}^2}t; \quad \eta_+=\frac{\eta}{D}; \quad R_+=\frac{R}{R_{\max}}, \tag{5}$$

Many authors [e.g., *Verhoest and Troch*, 2000] nondimensionalize the water table height by the depth of the aquifer; here we scale the water table height by its initial value and assume that the aquifer depth is great enough to contain all of the simulated water table heights. For the remainder of this derivation, we drop the subscripts for clarity and all variables will be dimensionless. The nondimensionalization transforms (3) into:

$$\frac{\partial\eta}{\partial t}=\frac{\partial^2\eta}{\partial x^2}+H_i\frac{\partial\eta}{\partial x}+H_rR(x,t), \tag{6}$$

with:

$$H_i=\frac{B_x\tan\theta}{\eta_0}, \quad H_r=\frac{{B_x}^2R_{\max}}{Dk_0\eta_0\cos\theta}. \tag{7}$$

The initial and boundary conditions must also be recast in dimensionless form:

$$\begin{aligned} &\text{dimensionless stream boundary condition}: \quad \eta=0 \quad x=0 \quad t\ge0,\\ &\text{dimensionless divide boundary condition}: \quad \frac{\partial\eta}{\partial x}+H_i\eta=0 \quad x=1 \quad t\ge0,\\ &\text{dimensionless initial condition}: \quad \eta=1 \quad 0\le x\le1 \quad t=0. \end{aligned} \tag{8}$$

Using the technique presented by *Guerrero et al*. [2009], we make the following substitution:

$$\eta(x,t)=u(x,t)\exp(at+bx), \tag{9}$$

$$a=-\frac{H_i^2}{4}, \quad b=-\frac{H_i}{2}. \tag{10}$$

With this substitution, (6) is transformed into a purely diffusive problem with a modified source term and boundary conditions:

$$\frac{\partial u}{\partial t}=\frac{\partial^2u}{\partial x^2}+\frac{H_rR(x,t)}{\exp(at+bx)}, \tag{11}$$

$$\begin{aligned} u=0 \quad x=0 \quad t \geq 0, \\ \frac{\partial u}{\partial x}+\frac{H_i}{2}u=0 \quad x=1 \quad t \geq 0, \\ u=\exp(-bx) \quad 0 \leq x \leq 1 \quad t=0. \end{aligned} \tag{12}$$

The Generalized Integral Transform Technique, which is related to the method of eigenfunction expansion, can be used to solve (11) [*Cotta*, 1993; *Mikhailov and Ozisik*, 1987]. The method of eigenfunction expansion is a standard solution method for partial differential equations, which we do not outline completely here. The reader is referred to *Haberman* [2012] for the details of this solution method.

We assume that any solution to (11) is separable and of the form:

$$u(x,t)=\sum_{m=1}^{\infty} c_m(t)\phi_m(x). \tag{13}$$

This separable solution can be obtained by first solving the eigen problem:

$$\frac{d^2\phi}{dx^2}+\lambda^2\phi=0. \tag{14}$$

Here ϕ and λ are the eigenfunction and eigenvalue of the boundary value problem associated with equation (11). For the fixed-interval boundary conditions listed in (12), equation (14) has eigenfunction solutions:

$$\phi_m=\sin(\lambda_m x) \quad m=1,2,3,..., \tag{15}$$

where the eigenvalues, λ_m, are the (infinitely many) transcendental roots of:

$$\lambda_m=-\frac{H_i \tan\lambda_m}{2} \quad \lambda_m>0 \quad m=1,2,3,... \tag{16}$$

The subscript m indicates that the eigen problem has a countably infinite number of solutions for the chosen boundary conditions, allowing one to find an infinite series solution for (11) in the form of equation (13). Substituting (13) into (11) yields:

$$\sum_{m=1}^{\infty}\frac{dc_m}{dt}\phi_m=\sum_{m=1}^{\infty}c_m\frac{d^2\phi_m}{dx^2}+\frac{H_r R}{\exp(at+bx)}. \tag{17}$$

With equation (14), equation (17) can be rewritten as:

$$\sum_{m=1}^{\infty}\left[\left(\frac{dc_m}{dt}+\lambda_m^2 c_m\right)\phi_m\right]=\frac{H_r R}{\exp(at+bx)}. \tag{18}$$

Multiplying (18) by ϕ_n and integrating from 0 to 1 causes all terms except for that with $m=n$ to go to zero (the orthogonality property of the eigenfunctions), yielding:

$$\frac{dc_n}{dt}+\lambda_n^2 c_n=\frac{\int_0^1\frac{H_r R}{\exp(at+bx)}\phi_n dx}{\int_0^1\phi_n^2 dx}=G(t). \tag{19}$$

Equation (19) requires an initial condition, which is obtained from the initial conditions of (11):

$$\sum_n c_n(0)\phi_n(x)=\exp(-bx). \tag{20}$$

Once again, the orthogonality property allows the series expansion to be evaluated:

$$\begin{aligned} C_n=c_n(0)&=\frac{\int_0^1\exp(-bx)\phi_n dx}{\int_0^1\phi_n^2 dx}, \\ &=\frac{4e^{-b}\lambda_n\left(b\sin(\lambda_n)+\lambda_n\left(\cos(\lambda_n)-e^b\right)\right)}{\left(b^2+\lambda_n^2\right)\left(\sin(2\lambda_n)-2\lambda_n\right)}. \end{aligned} \tag{21}$$

The solution to (19) is:

$$c_n(t) = \exp\left(-\lambda_n^2 t\right)\left[C_n + \int_0^t G(\tau)\exp\left(\lambda_n^2\tau\right)d\tau\right], \tag{22}$$

where τ is a dummy integration variable. Substituting (22) into (13) completes the solution for the transformed variable ($u(x,t)$). Using the variable transformation, equation (9), and the solution for $u(x,t)$, we can write the final, dimensionless solution for the water table height:

$$\eta(x,t) = \exp(at+bx)\sum_{n=1}^{\infty} c_n(t)\phi_n(x). \tag{23}$$

The volumetric outflow per length of channel q [L^2/T] can be computed from the water table profile using the linearized version the water table flux at any point along the hillslope [*Brutsaert*, 2005]; in dimensionless form (with the outflow scaled by $k_0\eta_0 D\cos\theta/B_x$), this is:

$$q = -\left(\frac{\partial\eta}{\partial x} + H_i\eta\right). \tag{24}$$

At the stream, the expression for dimensionless q simplifies to:

$$q_{stream} = -\frac{\partial\eta}{\partial x}. \tag{25}$$

Equation (25) represents the volume of water that is delivered to the adjacent stream per length of channel.

2.2. Incorporation of Spatio-Temporally Variable Recharge

The formulation of particular solutions for equation (22) is possible for a wide range of functional descriptions of the recharge dynamics in space and time ($R(x,t)$). Here we explore solutions that account for spatial variation of recharge as well as for variation of the total recharge volume in time due to the seasonality of rainfall or evaporation. To achieve this in general terms, we treat the recharge as a product of two functions, one of which varies in space and the other of which varies in time:

$$R(x,t) = M(t)N(x). \tag{26}$$

R is the total recharge normalized by its maximum rate, so $M(t)$ and $N(x)$ must be chosen to lie in the closed interval $[0,1]$. Substituting equation (26) into equation (19), the right hand side of (19) becomes:

$$\frac{\int_0^1 \frac{H_r M(t)N(x)}{\exp(at+bx)}\phi_n dx}{\int_0^1 \phi_n^2 dx} = \Phi_n M(t)e^{-at}, \tag{27}$$

with

$$\Phi_n = \frac{\int_0^1 H_r N(x)\exp(-bx)\phi_n dx}{\int_0^1 \phi_n^2 dx}. \tag{28}$$

The solution to equation (19) is then:

$$c_n(t) = \exp\left(-\lambda_n^2 t\right)\left[C_n + \Phi_n\int_0^t M(\tau)\exp\left(\lambda_n^2\tau - a\tau\right)d\tau\right], \tag{29}$$

where τ is again a dummy integration variable. Using equations (15), (23), and (25), the dimensionless expression for outflow at the stream is found as:

$$q_{stream} = -e^{at}\sum_n \lambda_n c_n(t) \tag{30}$$

Operationally, the solution can be implemented as follows: First, specify $M(t)$ and $N(x)$ (defined within the unit interval for dimensionless space and time variables) for the desired form of water table recharge. Next, integrate equation (28) using $N(x)$ to find Φ_n. Now substitute Φ_n and $M(t)$ into equation (29) to find the time dependent series coefficients ($c_n(t)$). With the eigenfunctions (ϕ_n) and the eigenvalues (λ_n) from equation

(16), substitute $c_n(t)$ into equation (23) to obtain the final (dimensionless) solution for the spatiotemporal evolution of the water table surface.

2.3. The Hillslope-Storage Boussinesq Equation

The solution methodology applied to equation (3) can also be used to find solutions to the more general linearized hillslope-storage Boussinesq equation [*Troch et al.*, 2003] which extends the LHB to account for topographic variation associated with hillslope divergence or convergence. As with the LHB, the LHSB equation is more tractable than the nonlinear form and has been solved for constant recharge [*Troch et al.*, 2004]. Here we briefly outline the solution method and solution obtained for the LHSB with spatiotemporally varying recharge. The LHSB takes the form:

$$\frac{\partial S}{\partial t}=K\frac{\partial^2 S}{\partial x^2}+U\frac{\partial S}{\partial x}+Rw, \tag{31}$$

where S [L^2] is soil moisture storage per longitudinal length of hillslope, R [L/T] is some spatiotemporally varying recharge term, and w [L], K [L^2/T], and U [L/T] are defined as:

$$w=ge^{hx}, \tag{32}$$

$$K=\frac{k_0\eta_0\cos\theta}{n_e}, \tag{33}$$

$$U=\frac{k_0\sin\theta-hk_0\eta_0\cos\theta}{n_e}. \tag{34}$$

Hillslope storage is directly related to water table height via the relation:

$$S(x,t)=n_e w(x)\eta(x,t). \tag{35}$$

The critical component of this reformulation is the hillslope width function (w), which prescribes the geometric width of the hillslope as a function of distance upslope (x). The parameters of the hillslope width function set the hillslope width at the stream boundary (the parameter g [L]) and the rate of increase or decrease of width moving in the upslope direction (the parameter h [1/L]). This allows for variable hillslope geometries (such as a divergent hillslope, where hillslope width (w) decreases with distance (x) from the stream, or a convergent hillslope where w increases with x) to be represented in a simple, one-dimensional Boussinesq framework. For constant hillslope width ($w=$ constant), the HSB simplifies to the HB.

We continue to adopt a zero head boundary at the stream, a no flux boundary at the upslope water table divide and a constant initial water table height above the bedrock as boundary conditions for the LHSB. Mathematically these conditions are expressed for the LHSB as:

$$\begin{aligned}&\text{stream boundary condition}: \quad S=0 \quad x=0 \quad t>0,\\ &\text{divide boundary condition}: \quad K\frac{\partial S}{\partial x}+US=0 \quad x=B_x \quad t>0,\\ &\text{initial condition}: \quad S=Dn_e ge^{hx} \quad 0\le x\le B_x \quad t=0.\end{aligned} \tag{36}$$

Again we consider spatiotemporally variable recharge of the form $R(x,t)=R_{max}M(t)N(x)$, and repeat the methods used to solve equation (3). This allows the following solutions to the LHSB to be found:

$$\begin{aligned}S(x,t)&=\exp(at+bx)\sum_{n=1}^{\infty}f_n(t)\psi_n(x),\\ a&=-\frac{U^2}{4K},\\ b&=-\frac{U}{2K},\end{aligned} \tag{37}$$

with

$$\psi_n=\sin(\mu_n x), \tag{38}$$

$$\frac{2K\mu_n}{U} = \tan(\mu_n B_x), \tag{39}$$

and

$$f_n(t) = \exp\left(-K\mu_n^2 t\right)\left[F_n + \Psi_n \int_0^t M(\tau)\exp\left(K\mu_n^2\tau - a\tau\right)d\tau\right], \tag{40}$$

with

$$\Psi_n = \frac{\int_0^{B_x} R_{\max} N w \psi_n e^{-bx} dx}{\int_0^{B_x} \psi_n^2 dx}, \tag{41}$$

and

$$F_n = \frac{4Dgn_e\mu_n\left(e^{(h-b)B_x}((h-b)\sin(B_x\mu_n) - \mu_n\cos(B_x\mu_n)) + \mu_n\right)}{\left((b-h)^2 + \mu_n^2\right)(2B_x\mu_n - \sin(2B_x\mu_n))}. \tag{42}$$

3. Validation of Analytical Solutions

In the supporting information, we test the solutions in three ways to ensure their applicability and validity when representing spatially variable recharge for both the HB and the HSB:

1. We compare our analytical solutions to previous analytical results obtained using the Laplace Transform method for spatially uniform recharge [*Verhoest and Troch*, 2000; *Troch et al*., 2003, 2004] and confirm that our solution exactly reproduces these previous results.
2. We compare analytical solutions of the LHB and LHSB with spatially variable recharge to numerical solutions of the LHB and LHSB equations obtained using a finite difference scheme [*Brutsaert*, 1994; *Verhoest and Troch*, 2000; *Troch et al*., 2003]. Our analytical solutions perfectly match the numerical solutions, confirming the correctness of our solutions for the previously unsolved case of spatially variable recharge. This item also provides a clear demonstration of the advantages of the analytical LHB solution: The numerical solution to the LHB equation took $\mathcal{O}(100)$ times longer to compute than the analytical solution, depending on the number of eigenvalues computed (for the analytical solution) and the grid size (for the numerical solution).
3. We compare the analytical solutions from the linearized equations to numerical solutions of the full nonlinear equations for equivalent boundary and initial conditions. This final test is intended to explore the validity of the linearization assumption in the context of abrupt changes in recharge fluxes through space, and in particular to determine whether or not large spatial gradients in recharge might induce large spatial gradients in the water table and violate the linearization assumption, $\left(\frac{\partial\eta}{\partial x}\right)^2 \approx 0$. We conclude that any additional error induced by the recharge pattern is negligible.

We find additional support for the third item in section 5.3, where we perform an in depth error analysis of the LHSB. The results show no significant error trend between the linear and nonlinear equations as the spatial pattern of recharge is varied, suggesting that the linearized equations appropriately capture hillslope sensitivity to recharge structure. Nevertheless, in agreement with *Troch et al*. [2003], we find that the absolute linearization error can be significant, especially on shallow, divergent slopes. *Troch et al*. [2003] also report that the choice of the mean water table height, η_0, can significantly alter the magnitude of the error. However, in this paper we only report linearization error sensitivity to hillslope geometry and recharge heterogeneity, leaving an analysis of the effects of the choice of the mean water table height for future work.

4. Modeling Scenarios

The solutions to the LHB and the LHSB outlined above were used to model three different scenarios of water table and base flow dynamics. In Scenarios 1 and 2, we explore two 'end member' cases, each of which divides a hillslope into two regions of homogenous recharge cover, with the extent of each region

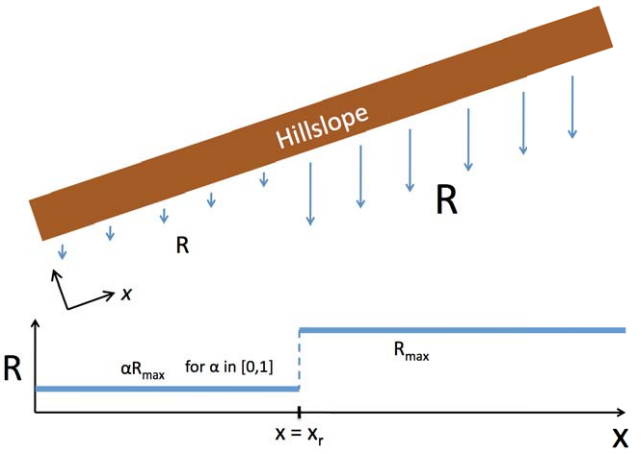

Figure 2. Illustration of the step function model for spatially variable water table recharge.

varying along the main hillslope axis (the 'x' axis in Figure 1). We assume that one of these recharge types occurs at a maximum dimensionless rate of $R = 1$ while the other is set to a fraction, α, of the maximum rate (for the purposes of our simulation, we set the low recharge to zero, $\alpha = 0$). An example of this type of recharge configuration is illustrated in Figure 2. We present analytical results for the case of an upslope step decrease in recharge and for an upslope step increase in recharge. These solutions are shown in Table 1. A third solution for a case in which recharge varies linearly with distance upslope is also presented in Table 1, but is not analyzed further. Scenario 1 compares the hillslope response to a pulse input of rainfall under different spatial distributions of recharge on linear hillslopes. Scenario 2 uses the same spatial recharge distributions, but explores their effects on water table and base flow variations on seasonal timescales, specifically during the transition from a wet season steady state condition to a dry season. A third scenario examines hillslope recession behavior, but in the context of the HSB model, allowing convergent and divergent hillslopes as well as linear hillslopes to be modeled.

4.1. Scenario 1: Effects of Spatially Heterogeneous Recharge on Storage-Discharge Responses to an Input Pulse of Water

The first model scenario addresses a recharge pulse lasting for 2 days entering dry hillslopes where the initial water table level is at the bedrock boundary ($\eta(x,0)=D=0$). Two cases are simulated: (i) upslope 50% high recharge and downslope 50% zero recharge, and (ii) upslope 50% zero recharge and downslope 50% high recharge. In both cases, the total hillslope integrated recharge per length of channel ($\int_0^{\beta_x} R(x,t)dx$) was fixed at 3.6 m^2/d during the 2 day pulse (this corresponds to a maximum recharge rate of 7.2 cm/d for the 100m long heterogeneously recharged hillslopes).

For each case, we examine two hillslopes (Hillslopes A and B in Table 2) with contrasting hydrogeologic characteristics. The specific parameterizations for this scenario are listed in Table 2, and the variety of observed dynamics can be interpreted using the scaling framework introduced in the derivation of equation (6). This

Table 1. Hillslope Boussinesq Dimensionless Forcing Functions for Linear Hillslopes With Recharge $R(x,t)=N(x)M(t)$[a]

N	Φ_n
$N_1(x)=\begin{cases}\alpha, & \text{if } 0\le x\le x_r\\ 1, & \text{if } x_r< x\le 1\end{cases}$	$\frac{4e^{-b(x_r+1)}H_r\lambda_n\left(b\left((\alpha-1)e^b\sin(x_r\lambda_n)+e^{bx_r}\sin(\lambda_n)\right)+\lambda_n\left(e^b\left((\alpha-1)\cos(x_r\lambda_n)-\alpha e^{bx_r}\right)+e^{bx_r}\cos(\lambda_n)\right)\right)}{\left(b^2+\lambda_n^2\right)(\sin(2\lambda_n)-2\lambda_n)}$
$N_2(x)=\begin{cases}1, & \text{if } 0\le x\le x_r\\ \alpha, & \text{if } x_r< x\le 1\end{cases}$	$-\frac{4e^{-b(x_r+1)}H_r\lambda_n\left(b\left((\alpha-1)e^b\sin(x_r\lambda_n)-\alpha e^{bx_r}\sin(\lambda_n)\right)+\lambda_n\left(e^b\left(e^{bx_r}+(\alpha-1)\cos(x_r\lambda_n)\right)-\alpha e^{bx_r}\cos(\lambda_n)\right)\right)}{\left(b^2+\lambda_n^2\right)(\sin(2\lambda_n)-2\lambda_n)}$
$N_3(x)=(1-\beta)x+\beta$	$\frac{4e^{-b}H_r\lambda_n\left(b^2(b-\beta+1)\sin(\lambda_n)+\lambda_n\left(-e^b\left(b((b-2)\beta+2)+\beta\lambda_n^2\right)+(b+\beta-1)\lambda_n\sin(\lambda_n)+\cos(\lambda_n)\left(b(b-2\beta+2)+\lambda_n^2\right)\right)\right)}{\left(b^2+\lambda_n^2\right)^2(\sin(2\lambda_n)-2\lambda_n)}$
M	$c_n(t)$
$M_1(t)=1$	$e^{-at}\left(C_n e^{at-t\lambda_n^2}-\Phi_n\frac{1-e^{at-t\lambda_n^2}}{a-\lambda_n^2}\right)$
$M_2(t)=\begin{cases}1, & \text{if } 0\le t\le t_d\\ \gamma, & \text{if } t> t_d\end{cases}$	$e^{-at}\left(C_n e^{at-t\lambda_n^2}-\Phi_n\frac{(\gamma-1)e^{-at_d+at+t_d\lambda_n^2-t\lambda_n^2}+e^{at-t\lambda_n^2}-\gamma}{\lambda_n^2-a}\right)$ valid for $t\ge t_d$
$M_3(t)=\begin{cases}\gamma, & \text{if } 0\le t\le t_d\\ 1, & \text{if } t> t_d\end{cases}$	$e^{-at}\left(C_n e^{at-t\lambda_n^2}+\Phi_n\frac{e^{-at_d+at+t_d\lambda_n^2-t\lambda_n^2}(\gamma-1)-\gamma e^{at-t\lambda_n^2}+1}{\lambda_n^2-a}\right)$ valid for $t\ge t_d$

[a]The forms of $c_n(t)$ displayed for $M=M_2(t)$ and $M_3(t)$ are only valid after the temporal transition at $t=t_d$; $x_r, \alpha, \beta, \gamma \in [0,1]$.

Table 2. Hillslope Parameterizations for Scenario 1

	Hillslope A	Hillslope B
Slope length (B_x) (m)	100	100
Slope angle (θ) (°)	0.1	6
Hydraulic conductivity (k_0) (m/d)	1000	86.4
Drainable porosity (n_e)	0.08	0.34
Mean water table height (η_0) (m)	0.67	0.67
Response timescale (t^*) (days)	4.58	3.76
Hillslope number (H_i)	0.26	15.78

nondimensionalization of the LHB yielded the dimensionless number, $H_i = \frac{B_x \tan\theta}{\eta_0}$, the so called "Hillslope number" [*Brutsaert*, 2005]. The Hillslope number is a type of Péclet number and therefore represents the relative strength of advective and diffusive behaviors. Additionally, we consider the absolute advective and diffusive response timescales for linear hillslopes. Following *Harman and Sivapalan* [2009], we examine $t^* = \frac{B_x n_e}{k_0 \sin\theta}$, which scales proportionally with both the advective ($\frac{t^*}{2}$) and diffusive ($\frac{t^*}{2\eta_0}$) response timescales for linear hillslopes. We use these similarity relationships to discuss the observed behaviors of Hillslopes A and B and to ensure that this study fully explores the variety of possible hillslope responses to spatially heterogeneous recharge.

4.2. Scenario 2: Effects of Recharge Spatial Distribution on Seasonal Storage-Discharge Responses in a Seasonally Dry Climate

The second model scenario addresses the effect of variable recharge on seasonal storage-discharge responses using a zeroth-order representation of recharge seasonality which mimics the canonical behavior of a seasonally dry climate. In such climates, rainfall events (and thus recharge) are concentrated over several months, which are followed by a prolonged dry season. The persistence of base flow supplied by discharge from groundwater and hillslope aquifers in the dry season has important implications for water resources and ecosystem health in seasonally dry climates [*Vico et al.*, 2014].

In this scenario, we explore the persistence of base flow from a hillslope aquifer as a function of recharge distribution for a step-decrease in recharge through time; represented by $M(t) = 1$ during the wet season (mathematically, we impose wet season conditions for $t < t_d$, where t_d is the seasonal transition time from wet to dry season) and $M(t) = 0$ during the dry season. Here $M(t) = 1$ represents a scenario where recharge occurs at the maximum rate specified by the spatial function $N(x)$. Again, analytical results for the water table dynamics are presented in Table 1 for this solution, as well as for temporally uniform recharge $M(t) = 1$ and for a step-increase in recharge in time from $M(t) = 0$ to $M(t) = 1$, providing a zeroth-order representation of the onset of the wet season. Equation (3) may also be solved for more complex forms of $M(t)$ (e.g., sinusoids), but the step functions used here capture the key features of a seasonal transition while maintaining as much analytical simplicity as possible.

To simulate hydrologic conditions at the end of a long wet season, we formulate the step function so that the maximum recharge rate is maintained until the water table and discharge approximate steady state conditions. We compute this time scale by noting that in the series solution for $\eta(x,t)$ it is the eigenvalues (λ_n) that control the rate at which the water table relaxes to its steady state condition. The dominant (smallest) eigenvalue (λ_1) characterizes the slowest of these transient dynamics. It provides a time scale $\tau = \frac{1}{\lambda_1^2}$ for this relaxation. By choosing the transition timescale in the step function (t_d) such that $t_d \gg \tau$, we ensure that the hillslope has reached a close approximation to its steady state wet season condition, and that the dynamics following the cessation of recharge reflect a realistic initial condition. This approach ensures that the initial water table profile during the seasonal transition is realistic [*Verhoest and Troch*, 2000], without having to rederive the analytical solution to equation (3) for a new suite of initial conditions. For Scenario 2, we choose $D = 1.5$ m, and, to ensure a steady state is reached, take $t_d = 1000$ days and set $M(t) = 0$ for $t > t_d$. For all cases modeled here, the pseudosteady water table approximated the true steady state condition to within 5% after 120 days, comparable to the response timescale for these hillslopes, $t^* \approx 112$ days. This indicates that these analyses are relevant in climates with long ($>$ 4 months) wet seasons. We impose the same recharge cases as those used in Scenario 1, where the recharge transition occurs at the hillslope midpoint, and present analyses for two hillslopes: a diffusion dominated hillslope (Hillslope 1) and an advection dominated hillslope (Hillslope 2). The specific parameterizations of Hillslopes 1 and 2 are listed in Table 3. The total hillslope integrated recharge rate is set to 1.5 m^2/d, corresponding to a maximum recharge rate of 1 cm/d on the 300m long heterogeneously recharged hillslopes.

4.3. Scenario 3: Topographically Variable Hillslopes

In this scenario we explore the interplay between recharge and hillslope morphology by varying the parameter h in the hillslope width function from $h = -0.03$ to $h = 0.03$ (very divergent to very convergent hillslopes) and

Table 3. Hillslope Parameterizations for Scenario 2

	Hillslope 1	Hillslope 2
Slope length (B_x) (m)	300	300
Slope angle (θ) (°)	0.1	6
Hydraulic conductivity (k_0) (m/d)	230	8.64
Drainable porosity (n_e)	0.15	0.34
Mean water table height (η_0) (m)	0.67	0.67
Response timescale (t^*) (days)	112.10	112.94
Hillslope number (H_i)	0.78	47.29

varying the extent of the downslope fraction of the hillslope which receives zero recharge (from 0 to 75%). The analytical results for the LHSB for the case of high upslope recharge are shown in Table 4. We again compute the water table and discharge dynamics over a step-decrease in recharge in time at $t = 1000$ days (to ensure that steady state conditions are achieved before the onset of recession).

We control for the total input volume of recharge by firstly controlling for the total hillslope area as the hillslope width function ($w = ge^{hx}$) changes (we fix this area as $A = 2000$ m^2), and then adjusting the maximum recharge rate to fix the total recharge volume entering the hillslope at 20 m^3/d. Hillslope convergence is varied with the exponential parameter (h) in the hillslope width function (w), constraining the other hillslope width parameter (g):

$$A = \int_0^{B_x} w(x)dx = \int_0^{B_x} ge^{hx}dx \;\rightarrow\; g = \frac{Ah}{e^{B_x h} - 1} \tag{43}$$

We parameterize the LHSB model as follows: hillslope length $B_x = 100$ m; hydraulic conductivity $k_0 = 1$ m/hr; drainable porosity $n_e = 0.30$; initial water table height $D = 0.4$ m and mean water table height $\eta_0 = 0.9$ m. We run the simulations for two hillslope angles: 5° and 15°. For complex hillslopes such as these, *Troch et al.* [2004] follow *Brutsaert* [1994] and suggest a type of Péclet number:

$$H_{\text{topo}} = \frac{B_x \tan\theta}{2\eta_0} - \frac{hB_x}{2}, \tag{44}$$

which is analogous to the Hillslope number (H_i) for topographically complex hillslopes with exponential width functions (h is the exponential rate of convergence or divergence of the hillslope width function). For $h \in [-0.03, 0.03]$ m^{-1} and $\theta \in [5^\circ, 15^\circ]$, H_{topo} ranges from 3.36 (for shallow, highly convergent hillslopes) to 16.38 (for steep, highly divergent hillslopes), indicating that these hillslopes are advection dominated.

In this scenario, we allow the water table to approach a steady state condition and then 'turn off' recharge completely and compute the e-folding time (the recession constant, or the time required for outflow to decline to $\frac{1}{e}$ of its original value) for the flow recession curve. We propose this e-folding recession time as representative of the storage and discharge variability between different topography-recharge combinations. The linearization of HSB, however, requires more simplifying assumptions (as compared to the linearized HB) and therefore introduces errors that can significantly affect single-valued flow recession metrics, such as the e-folding time. To assess the validity of the LHSB for measuring flow recession characteristics, we also calculate the e-folding recession time for select hillslopes using the full, nonlinear HSB equation. With this, we compute linearization error surfaces for the e-folding time across a variety of hillslopes.

5. Results

5.1. Scenario 1: Effects of Recharge Spatial Distribution on Storage-Discharge Responses to an Input Pulse of Water

The hillslope discharge per length of channel induced by a 2 day water pulse recharging a dry water table is shown as a function of time for high upslope and downslope recharge on Hillslopes A and B in Figures 3a

Table 4. Hillslope-Storage Boussinesq Forcing Function for Complex Hillslopes With Recharge $R(x,t) = R_{\max} N(x) M(t)$[a]

N	Ψ_n
$N(x) = \begin{cases} \alpha, & \text{if } 0 \le x \le x_r \\ 1, & \text{if } x_r < x \le B_x \end{cases}$	$\begin{cases} 4gR_{\max}\mu_n\{(b-h)(e^{(h-b)B_x}\sin(B_x\mu_n) + (\alpha-1)e^{(h-b)x_r}\sin(\mu_n x_r)) \\ +\mu_n(-\alpha + e^{(h-b)B_x}\cos(B_x\mu_n) + (\alpha-1)e^{(h-b)x_r}\cos(\mu_n x_r))\} \\ /\{((b-h)^2+\mu_n^2)(\sin(2B_x\mu_n) - 2B_x\mu_n)\} \end{cases}$
M	$f_n(t)$
$M(t) = \begin{cases} 1, & \text{if } 0 \le t \le t_d \\ \gamma, & \text{if } t > t_d \end{cases}$	$e^{at}\left(F_n e^{at - Kt\mu_n^2} + \Psi_n \frac{\gamma e^{at - Kt\mu_n^2} - e^{Kt_d\mu_n^2 - at_d + at - Kt\mu_n^2} + e^{at - Kt\mu_n^2} - \gamma}{a - K\mu_n^2}\right)$ valid for $t \ge t_d$

[a]The form of $f_n(t)$ displayed is only valid after the temporal transition at $t = t_d$; $x_r \in [0, B_x]$ and $\alpha, \gamma \in [0, 1]$.

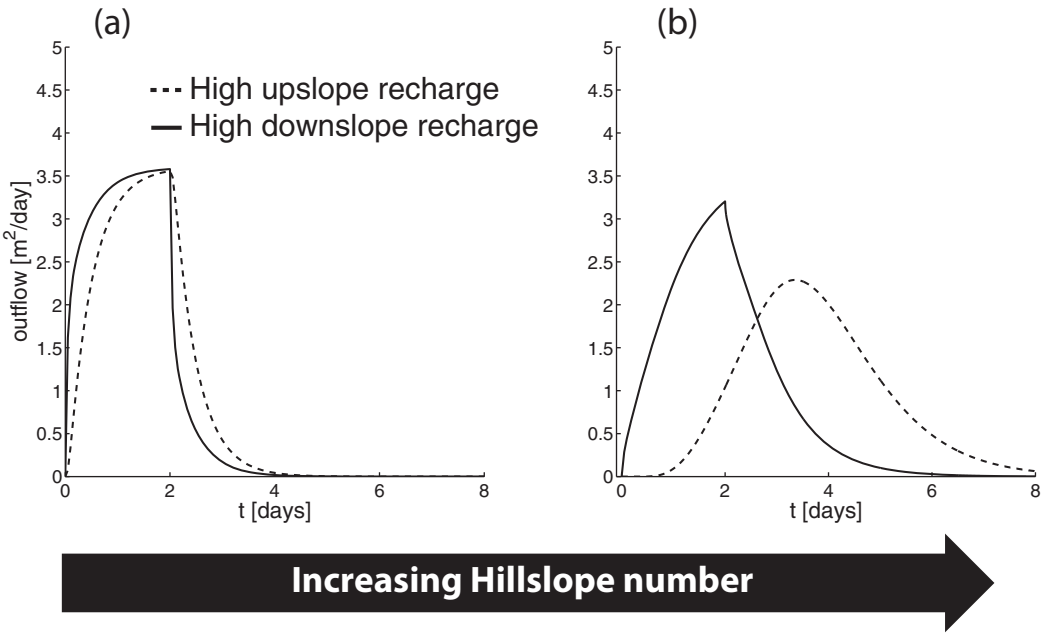

Figure 3. Outflow response to a 2 day pulse of recharge ($M = M_2$, $\gamma = 0$, $t_d = 2$ days) for Hillslopes (a) A and (b) B. Dashed lines illustrate results for high upslope recharge ($N = N_1$, $x_r = 50$m, $\alpha = 0$, $R_{max} = 7.2$ cm/d) and solid lines for high downslope recharge ($N = N_2$, $x_r = 50$m, $\alpha = 0$, $R_{max} = 7.2$ cm/d).

and 3b, respectively. Although both hillslopes receive and eventually discharge the same total volume of water, the spatial location of recharge and the hydrogeologic character of the hillslopes clearly alter the peak flow and timing of this discharge. For Hillslope B (advection dominated), high upslope recharge exhibits a large lag between the cessation of recharge and the timing of peak flow (as compared to high downslope recharge). In contrast, Hillslope A (diffusion dominated) exhibits an insignificant lag in peak flow after the cessation of recharge under both high upslope and high downslope recharge. High downslope recharge produces a more rapid response on both Hillslopes A and B, although the peak size for high downslope recharge relative to the peak size for high upslope recharge strongly depends on the advective/diffusive characteristics of the hillslope. Peak discharge values are primarily driven by response time, and vary from 3.58 m^2/d for high downslope recharge on Hillslope A to 2.29 m^2/d for high upslope recharge on Hillslope B.

5.2. Scenario 2: Effects of Recharge Spatial Distribution on Seasonal Storage-Discharge Responses in a Seasonally Dry Climate

Steady state water table profiles for Hillslopes 1 and 2 are illustrated in solid lines in Figures 4a, 4b, 4d, and 4e, respectively. For each hillslope, snapshots of the water table drawdown are shown for times $t = 20, 50,$ and 100 days following both a seasonal high upslope recharge event (Figures 4a and 4d) and a seasonal high downslope recharge event (Figures 4b and 4e). It is clear that the steady state storage profiles are strongly influenced by the recharge distribution, with generally higher steady state storage for the cases of high upslope recharge. Following the cessation of recharge, each of these water tables drains to the channel, generating the outflow recession curves plotted in Figures 4c and 4f. As a consequence of the enforced steady state condition and equivalent hillslope total recharge volume in the model runs, the initial outflows from all four simulations are the same ($q = 1.5$ m^2/d). As the hillslopes begin to drain, however, the outflow curves diverge from each other. For the cases of high upslope recharge, steady state storages are larger and thus outflows tend to recess more slowly than for the high-downslope recharge profiles.

5.3. Scenario 3: Topographically Variable Hillslopes

Figures 5a and 5d present contours of the recession constant (*e*-folding time) for different hillslope geometries and recharge extents using the LHSB. Figures 5a and 5d indicate that the influence of recharge variability on discharge is maximized in divergent hillslopes. At larger hillslope angles, however, the contours are

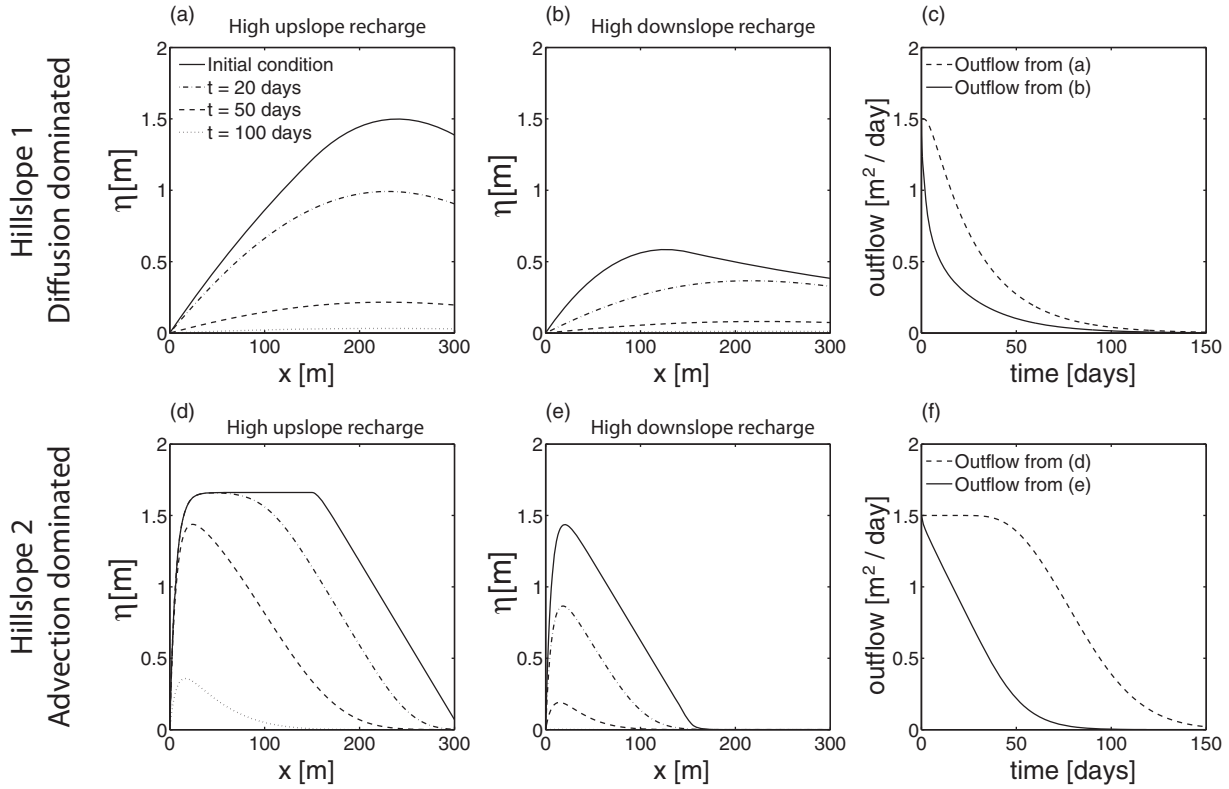

Figure 4. Recessions from steady state water table profiles for Hillslopes 1 and 2 for (a, d) high upslope recharge and(b, e) for high downslope recharge. Forcing functions are obtained from Table 1 letting $M = M_2$, $\gamma = 0$, $t_d = 1000$ days with $N = N_1$, $x_r = 150$ m, $\alpha = 0$ for high upslope recharge (Figures 4a and 4d) and $N = N_2$, $x_r = 150$ m, $\alpha = 0$ for high downslope recharge (Figures 4b and 4e). Water table profiles are plotted at 0, 20, 50, and 100 days after the cessation of recharge. The outflows corresponding to the draining water table profiles are plotted in Figures 4c and 4f, where time is in days after the dry-down transition ($t = t_d$) at 1000 days.

generally parallel, meaning that steep divergent and convergent slopes are comparably sensitive to recharge heterogeneity.

Figures 5c and 5f replicate the recession contours presented in Figures 5a and 5d except that the contours are calculated using a numerical solution of the full nonlinear HSB. Qualitatively, trends in the *e*-folding recession time using the nonlinear HSB match the plots created using the linearized equation. Error surfaces (Figures 5b and 5e) demonstrate that the accuracy of the LHSB depends only somewhat on the spatial character of recharge and strongly on the hillslope morphology. Relative error is largest in shallow divergent hillslopes, in agreement with error trends found by *Troch et al.* [2003] for hillslopes with spatially homogeneous recharge.

6. Discussion

6.1. Spatially Heterogeneous Recharge Effects on Water Storage and Runoff Generation

All three scenarios demonstrate that the spatial distribution of recharge could significantly alter the hillslope water table profile as well as the temporal character of hillslope discharge. It is apparent that topography and the hydrogeologic character of a given hillslope mediate the impact of spatially heterogeneous recharge, resulting in diverse subsurface storage and discharge behaviors.

6.2. Scenario 1

The results of Scenario 1, the case of a pulse input of water to the subsurface, suggest that (all other factors being equal) hillslopes with lower downslope recharge (relative to upslope recharge) are likely to exhibit longer lags between a rainfall input and the peak of base flow response. We find that these slopes exhibit lower peak flow rates and longer base flow persistence compared to hillslopes where recharge is concentrated downslope. Additionally, increased travel time for water entering the groundwater store upslope

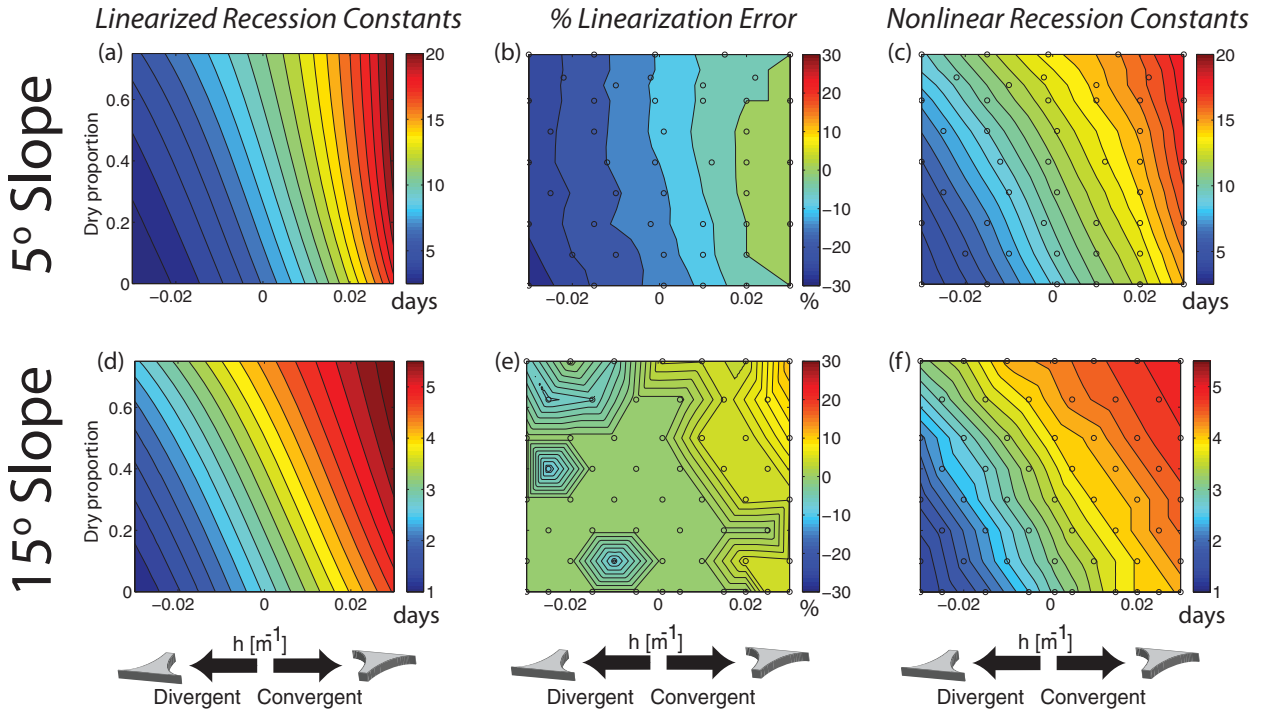

Figure 5. Contour plots of recession constants for (a, d) the linearized HSB simulations and(c, f) the nonlinear HSB for varying recharge distributions and hillslope geometries (calculated using Table 4 with $t_d = 1000$ days, $\gamma = 0$, $\alpha = 0$). Circles on the contour plot indicate the parameter combinations for which the nonlinear HSB was numerically solved. The vertical axis in Figures 5a, 5c, 5d, and 5f indicates the downslope proportion (by area) of the hillslope that receives no recharge. The horizontal axis indicates the strength of hillslope convergence or divergence, as measured by the parameter h in the hillslope width function (w). The illustrated hillslopes on the horizontal axis correspond in scale to approximately $h = 0.02$ (convergent) and $h = -0.02$ (divergent). The recharge rate on homogeneously recharged hillslopes (dry proportion $=0$) is 10 mm/d and the slope length $B_x = 100$ m. Figures 5b and 5e contour the percent error of the recession constant computed by the linearized HSB against the recession constant computed by the nonlinear HSB.

increases the amount of time available for diffusion, resulting in enhanced dispersion of the discharge response.

The scaling framework of *Harman and Sivapalan* [2009] provides a more thorough interpretation of the variety of behaviors exhibited in the plots of Figure 3. For example, the highly diffusive (low Hillslope number) nature of Hillslope A leads to a discharge response that appears to have little sensitivity to the spatial structure of the recharge. Hillslope A also has a rapid response timescale (low t^*) and drains nearly all of its stored water within 4 days of the recession onset. The result is a discharge signal that responds rapidly, exhibiting only minor differences between the cases of high upslope recharge and high downslope recharge. In comparison, Hillslope B responds on a time scale comparable to Hillslope A, but the advective nature of the hillslope (higher Hillslope number) leads to greater preservation of the spatial structure of the recharge signal, leading to a lagged response for uphill recharge. These results are characteristic of most advective-diffusive systems; diffusion tends to dampen spatial heterogeneity while advection serves to preserve it. Given that the advective nature of a hillslope is proportional to hillslope length and the tangent of the hillslope angle ($H_i = \frac{B_x \tan\theta}{\eta_0}$), we conclude that recharge heterogeneity at event time scales is the most hydrologically relevant on long, steep hillslopes.

6.3. Scenario 2

Under steady state recharge conditions (Scenario 2), it is evident that the spatial pattern of recharge places a strong control on the volume and profile of storage in the water table (Figure 4). Where recharge primarily occurs upslope, the whole hillslope is available for water storage, increasing total storage at steady state. Recharge that occurs primarily downslope is effectively stored in a smaller volume of soil, since groundwater movement in the upslope direction is limited, and the connection to the channel over a relatively short distance reduces the volumetric storage needed to achieve the hydraulic gradients for steady state outflow conditions.

Although recharge heterogeneity significantly alters the spatial structure of steady state storage, the relative strengths of hillslope advective and diffusive behaviors mediate the strength of its impact. For example, in Hillslope 1 (a diffusion dominated hillslope) storage is more evenly dispersed in the subsurface at steady

state due to the hillslope's low topographic gradient. The steep topographic gradients in Hillslope 2, however, restrict the spatial redistribution of storage, leading to groundwater piling near the outlet. This is characteristic of strongly advective hillslopes. Thus, storage is more evenly distributed throughout Hillslope 1 for both upslope and downslope high recharge, while in Hillslope 2, storage is limited to the lower half of the hillslope for the case of high downslope recharge.

Figures 4c and 4f indicate that these storage effects are propagated into the recession hydrographs. The results indicate that base flow is more likely to persist from hillslopes with higher upslope recharge than hillslopes with higher downslope recharge under equivalent climatic forcing. This effect is weaker in Hillslope 1 due to greater storage redistribution. In Hillslope 2, there is a greater disparity in total storage between the cases of high upslope recharge and high downslope recharge. The steady state storage profiles of Hillslope 2 are preserved by its advective nature, resulting in a large lag before any significant recession of flow for the case of high upslope recharge.

6.4. Scenario 3

In order to explore the potential effects of heterogeneous recharge on the hydrology of topographically complex hillslopes, we compared the hillslope outflow recession constant over a range of recharge patterns and hillslope geometries. Figure 5 suggests that specific changes in recharge spatial structure may lead to near-equivalent recession behavior between hillslopes with different topographic characteristics. For example, the recession constants are equivalent between a highly convergent ($h \approx 0.02$), 15° angled hillslope with homogeneous recharge and a linear, 15° angled hillslope with the upper half of its surface receiving high recharge. The steady state volume of hillslope water storage (not shown) was found to follow nearly the same pattern as the recession constant, with larger storage volumes corresponding to longer recessions. The spatial distribution of recharge was also shown to amplify or dampen the effects of hillslope morphology. Increasing convergence increases hillslope storage at steady state, which leads to longer recessions. The effect is similar for an increase in the downslope portion of a hillslope that receives low recharge. In other words, reducing the amount of recharge downslope appears to diminish the divergent character or enhance the convergent character of a hillslope. The relative effects, however, of spatially heterogeneous recharge are less important on more diffusive hillslopes, as evidenced by the steeper contour slopes in Figure 5a. Although, increasing divergence can counteract the effects of diffusion by increasing the advective nature of the hillslope (according to equation (44)), preserving more of the recharge structure in the discharge signal. We conclude that steep, divergent hillslopes are most affected (in the relative sense) by spatially heterogeneous recharge.

To evaluate the effects of the linearization assumptions on the computed *e*-folding times, we repeated the analysis using the full nonlinear HSB. The general trend of increasing recession time for increasing hillslope convergence remains the same using the full HSB. Error surfaces demonstrate that the LHSB successfully captures the strength of this trend on the 15° hillslope. On the 5° hillslope, the trend is captured on all slopes but absolute accuracy erodes for increasingly divergent hillslopes. The error is increasingly negative for decreasing h, showing that the LHSB underestimates the actual recession timescale.

The effects of increasing recharge heterogeneity are appropriately captured on both the steep and shallow hillslopes. Although the absolute error is significant for the 5° hillslope, there is essentially no trend in the error with changing the extent of the hillslope that receives zero recharge. Error on the 15° hillslope exhibits no strong trend and appears to be quite noisy, presumably due to numerical error in the solution of the nonlinear HSB. This suggests that for these hillslopes, linearization and numerical approximations may contribute comparably significant errors.

Although it is clear from Figure 5 that topography remains the dominant driver of steady state storage and recession timing, the effects of recharge spatial distribution are not negligible and could be very significant. Recession constant trends calculated using both the nonlinear and linearized HSB indicate that hillslopes with more recharge heterogeneity generally exhibit longer recession timescales with a stronger relative effect on steep, divergent hillslopes. For the purposes of modeling, however, these simulations also suggest that the LHSB should be used with caution.

6.5. Model Limitations

Clearly this theoretical study has numerous limitations in terms of its realistic representation of the spatial character of recharge to the water table. Variations in net recharge to unconfined hillslope aquifers are not

empirically quantified and may be offset by heterogeneity in other hydrogeological characteristics (e.g., soil depth, bedrock slope, bedrock topography, porosity, or hydraulic conductivity) that are not considered.

The analysis is also limited by the assumptions and linearization of the hillslope Boussinesq equation, which introduce varying degrees of error for water table and outflow predictions. *Troch et al*. [2013] provide review of the problems and benefits associated with the use of the Boussinesq approach.

Despite these limitations, the study goals — to explore the potential for spatially organized recharge patterns to alter hydrology — are reasonably met by the simplified spatiotemporal dynamics, which capture the gross features of spatial variation in recharge patterns and temporal variation in recharge due to seasonality that influences many real systems. With this in mind, we propose avenues for future work.

7. Future Work

Further pursuit of our guiding motivation — to understand the hydrologic impact of spatially variable vegetation cover in catchments with significant subsurface lateral transport — leads to several potential theoretical and empirical extensions of this work. Coupled with a realistic representation of the dynamics of vegetation and the unsaturated zone, the analytical approaches here suggest that there may be ways to rapidly iterate toward solutions for coupled vegetation-water table profile dynamics, and to explore different optimization and competition schemes in comparison with real-world observations. To justify more complex extensions of this work, however, there is a need to evaluate both model assumptions and model predictions in real systems. The quantification of recharge rates (and potentially net uptake from water tables, which can be easily fit into these equations as a negative $R(x, t)$ value) between different forms of co-occurring vegetation cover types is required. Observational data of water table dynamics along hillslopes with varying vegetation properties would further illuminate the subsurface response to surface heterogeneities. At the basin scale, paired catchment experiments where different spatial patterns of vegetation cover are experimentally imposed may exhibit some of the behaviors simulated in this theoretical study.

8. Conclusion

This study developed a novel and (comparatively) straightforward analytical solution approach to the linearized hillslope Boussinesq and hillslope-storage Boussinesq equations. Our simple simulations demonstrate that, in conjunction with hillslope topography, the spatial distribution of water table recharge may cause a nontrivial modification of catchment storage and discharge responses on multiple time scales. We hypothesize that vegetation has the potential to alter the spatial character of recharge and suggest the Boussinesq framework as a promising avenue for the development of new hillslope-scale ecohydrologic theory.

Acknowledgments
D. Dralle thanks the NSF GRFP. S.E. Thompson acknowledges support from the National Science Foundation CZP EAR-1331940 for the Eel River Critical Zone Observatory.

References

Boussinesq, J. (1877), *Essai sur la Théorie des Eaux Courantes*, vol. 2, Imprimerie Natl., Paris, France.
Brutsaert, W. (1994), The unit response of groundwater outflow from a hillslope, *Water Resour. Res.*, *30*(10), 2759–2763, doi:10.1029/94WR01396.
Brutsaert, W. (2005), *Hydrology: An Introduction*, Cambridge Univ. Press, Cambridge, U. K.
Cotta, R. M. (1993), *Integral Transforms in Computational Heat and Fluid Flow*, CRC Press, Boca Raton, Fla.
Guerrero, J. S. P., L. C. G. Pimentel, T. H. Skaggs, and M. T. van Genuchten (2009), Analytical solution of the advection-diffusion transport equation using a change-of-variable and integral transform technique, *Int. J. Heat Mass Transfer*, *52*(13-14), 3297–3304.
Haberman, R. (2012), *Applied Partial Differential Equations With Fourier Series and Boundary Value Problems*, Pearson, Upper Saddle River, N. J.
Harman, C., and M. Sivapalan (2009), A similarity framework to assess controls on shallow subsurface flow dynamics in hillslopes, *Water Resour. Res.*, *45*, W01417, doi:10.1029/2008WR007067.
Hilberts, A. G. J., P. A. Troch, C. Paniconi, and J. Boll (2007), Low-dimensional modeling of hillslope subsurface flow: Relationship between rainfall, recharge, and unsaturated storage dynamics, *Water Resour. Res.*, *43*, W03445, doi:10.1029/2006WR004964.
Huyck, A. A. O., V. R. N. Pauwels, and N. E. C. Verhoest (2005), A baseflow separation algorithm based on the linearized Boussinesq equation for complex hillslopes, *Water Resour. Res.*, *41*, W08415, doi:10.1029/2004WR003789.
Mikhailov, M. D., and M. N. Ozisik (1987), Unified analysis of solute diffusion with reversible reaction, *J. Appl. Phys.*, *62*(8), 3184–3189.
Pauwels, V. R., N. E. Verhoest, and F. P. De Troch (2002), A metahillslope model based on an analytical solution to a linearized Boussinesq equation for temporally variable recharge rates, *Water Resour. Res.*, *38*(12), 1297, doi:10.1029/2001WR000714.
Polubarinova-Kochina, P. I. (1962), *Theory of Ground Water Movement*, Princeton Univ. Press, Princeton, N. J.
Rupp, D. E., J. Schmidt, R. A. Woods, and V. J. Bidwell (2009), Analytical assessment and parameter estimation of a low-dimensional groundwater model, *J. Hydrol.*, *377*(1-2), 143–154, doi:10.1016/j.jhydrol.2009.08.018.
Troch, P. A., C. Paniconi, and E. Emiel van Loon (2003), Hillslope-storage Boussinesq model for subsurface flow and variable source areas along complex hillslopes: 1. Formulation and characteristic response, *Water Resour. Res.*, *39*(11), 1316, doi:10.1029/2002WR001728.

Troch, P. A., A. H. Van Loon, and A. G. J. Hilberts (2004), Analytical solution of the linearized hillslope-storage Boussinesq equation for exponential hillslope width functions, *Water Resour. Res.*, *40*, W08601, doi:10.1029/2003WR002850.

Troch, P. A., et al. (2013), The importance of hydraulic groundwater theory in catchment hydrology: The legacy of Wilfried Brutsaert and Jean-Yves Parlange, *Water Resour. Res.*, *49*, 1–18, doi:10.1002/wrcr.20407.

Verhoest, N. E. C., and P. A. Troch (2000), Some analytical solutions of the linearized Boussinesq equation with recharge for a sloping aquifer, *Water Resour. Res.*, *36*(3), 793–800, doi:10.1029/1999WR900317.

Vico, G., et al. (2014), On the interplay among climate, ecophysiological traits and leaf phenology inshaping plant ecohydrological strategies in seasonally dry ecosystems, *Ecohydrology*, doi:10.1002/eco.1533.

Woods, R. A., M. Sivapalan, and J. S. Robinson (1997), Modeling the spatial variability of subsurface runoff using a topographic index, *Water Resour. Res.*, *33*(5), 1061–1073, doi:10.1029/97WR00232.